Model Predictive Torque and Flux Control Minimizing Current Distortions

Petros Karamanakos, *Member, IEEE*, and Tobias Geyer, *Senior Member, IEEE*

Abstract—A new model predictive torque and flux controller is proposed, which controls the electromagnetic torque and the rotor (rather than the stator) flux magnitude. Analytical expressions for the weighting factors are derived that ensure that the proposed controller achieves the same closed-loop performance as predictive current control. In particular, the same low current and torque distortions result, without requiring an outer field-oriented control loop.

Index Terms—Model predictive control, finite control set, cost function, penalty weights, tuning, torque and flux control, current control, power converters, variable speed drives.

I. INTRODUCTION

Model predictive torque and flux control (MPTFC) is a direct control method, i.e., it does not require a modulator [1]. The control objective is to regulate the two main quantities of an electrical machine—the electromagnetic torque and the magnetization of the machine—along their reference values. To this aim, a corresponding objective function is minimized online subject to an inverter and machine model. This yields the optimal switch position (i.e., the control input) which is applied to the power converter [2].

The design simplicity, the straightforward implementation, and the intuitive concept are among the advantages of this model predictive control (MPC) method. Moreover, akin to direct torque control (DTC) [3], fast transients are achieved. On the downside, the choice of the weighting factors—and thus the tuning procedure—may be difficult, because one has to decide on the relative importance between the torque error and the flux magnitude error. This also affects the current distortions, which are typically higher than with model predictive current control (MPCC) [2], [4].

The recent paper [5] provides a first insight into MPTFC. Therein, the value of the weighting factors that minimize the current distortions are analytically derived. However, MPCC [6] still achieves lower current distortions, particularly at non-zero torque references and low switching frequencies. As shown in [5], this difference results from the different shape of the level sets of the objective functions of the two controllers; the level sets of MPTFC are elliptical in contrast to the circular ones of MPCC.

This paper proposes a slight modification to MPTFC. By tracking the *rotor* instead of the stator flux magnitude, MPTFC is made *equivalent* to MPCC with *circular* level sets. As a

P. Karamanakos (corresponding author) is with the Faculty of Computing and Electrical Engineering, Tampere University of Technology, 33101 Tampere, Finland; e-mail: p.karamanakos@ieee.org

T. Geyer is with ABB Corporate Research, 5405 Baden-Dättwil, Switzerland; e-mail: t.geyer@ieee.org

result, both controllers issue the same switching sequences and achieve the same current and torque trajectories. With this new approach, the advantages of MPTFC remain in place. Among them, there is no need for a field-oriented control loop to adjust the current references in a rotating reference frame, which greatly simplifies the design procedure. As with conventional model predictive torque control [1], [5], however, the proposed MPTFC requires rotor parameters.

Normalized quantities are used throughout the paper. To this end, we introduce a per unit system using as base quantities the peak value of the rated phase voltage of the machine, the peak value of the rated machine current, and the rated fundamental frequency. Moreover, all variables $\boldsymbol{\xi}_{abc} = [\xi_a \ \xi_b \ \xi_c]^T$ in the three-phase (abc) system are mapped into the variables $\boldsymbol{\xi}_{dq} = [\xi_d \ \xi_q]^T$ in the dq plane, which is an orthogonal, two-dimensional coordinate system that rotates with the angular speed ω_{fr}. We define $\boldsymbol{\xi}_{dq} = \boldsymbol{K}(\varphi)\boldsymbol{\xi}_{abc}$, where φ is the angle between the d- and the a-axis. If the orthogonal plane is stationary ($\omega_{\mathrm{fr}} = 0$), then the plane is referred to as the $\alpha\beta$ plane, and the performed mapping is $\boldsymbol{\xi}_{\alpha\beta} = \boldsymbol{K}(0)\boldsymbol{\xi}_{abc}$, with $\boldsymbol{\xi}_{\alpha\beta} = [\xi_\alpha \ \xi_\beta]^T$. Vectors in the abc and dq planes are denoted with the corresponding subscript. For vectors in the $\alpha\beta$ plane, the subscript is omitted.

II. MODELING

Consider a variable speed drive based on a three-level neutral point clamped (NPC) inverter and an induction machine (IM). To simplify the analysis presented hereafter, the neutral point potential is assumed to be fixed and equal to zero. The dynamics of the squirrel-cage IM can be described in terms of the stator current vector $\boldsymbol{i}_s$ and the stator flux linkage vector $\boldsymbol{\psi}_s$. The differential equations of interest can be derived based on the so-called T-equivalent circuit of a squirrel-cage IM, see Fig. 1. The differential equations are [7]

$$\frac{\mathrm{d}\boldsymbol{i}_s}{\mathrm{d}t} = \left(\omega_r \boldsymbol{Q} - \frac{\Phi}{D}\boldsymbol{I}\right)\boldsymbol{i}_s + \left(\frac{R_r}{D}\boldsymbol{I} - \omega_r \boldsymbol{Q}\frac{X_r}{D}\right)\boldsymbol{\psi}_s + \frac{X_r}{D}\boldsymbol{v}_s \tag{1a}$$

$$\frac{\mathrm{d}\boldsymbol{\psi}_s}{\mathrm{d}t} = -R_s \boldsymbol{i}_s + \boldsymbol{v}_s \,, \tag{1b}$$

where ω_r is the electrical angular speed of the rotor. The machine parameters are the stator R_s and rotor R_r resistances, as well as the stator X_{ls}, rotor X_{lr} and mutual X_m reactances. Based on these, the stator and rotor self-reactances are defined as $X_s = X_{ls} + X_m$ and $X_r = X_{lr} + X_m$, respectively. We also define $\Phi = R_s X_r + R_r X_s$, $D = X_s X_r - X_m^2$, $\boldsymbol{Q} = \begin{bmatrix} 0 & -1 \\ 1 & 0 \end{bmatrix}$, and the two-dimensional identity matrix $\boldsymbol{I}$.
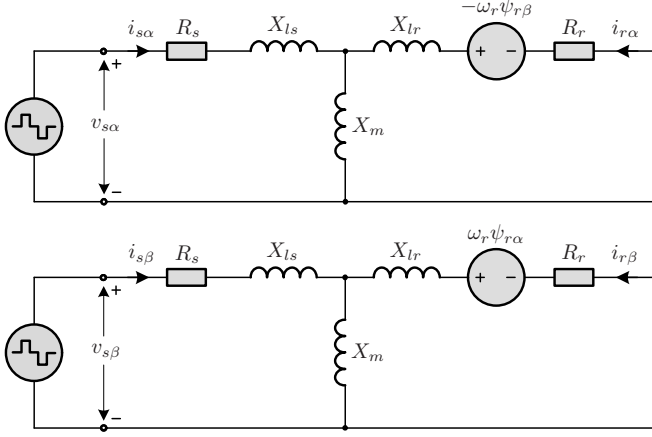
Fig. 1: T-equivalent circuit representation of a squirrel-cage induction machine driven by a three-level neutral point clamped inverter in the $\alpha\beta$ plane (top: α-axis, bottom: β-axis).

The output voltage of the inverter is equal to the stator voltage

$$\boldsymbol{v}_s = \frac{V_{\mathrm{dc}}}{2} \boldsymbol{K}(0)\boldsymbol{u}_{abc}, \qquad (2)$$

with V_{dc} being the dc-link voltage and $\boldsymbol{u}_{abc} = [u_a\ u_b\ u_c]^T \in \mathcal{U} = \mathcal{U}^3$ the *three-phase* switch position. The *single-phase* switch position $u_x \in \mathcal{U}$, with $x \in \{a,b,c\}$, assumes integer values depending on the output voltage levels of the inverter. For a three-level NPC inverter, e.g., we have $\mathcal{U} = \{-1,0,1\}$.

The electromagnetic torque T_e can be expressed in terms of the state variables as

$$T_e = \frac{1}{\mathrm{pf}} \boldsymbol{\psi}_s \times \boldsymbol{i}_s = \frac{1}{\mathrm{pf}}(\psi_{s\alpha} i_{s\beta} - \psi_{s\beta} i_{s\alpha}), \qquad (3)$$

where pf denotes the power factor.

We define the state vector $\boldsymbol{x} = [i_{s\alpha}\ i_{s\beta}\ \psi_{s\alpha}\ \psi_{s\beta}]^T \in \mathbb{R}^4$, and the three-phase switch position as the system input $\boldsymbol{u} = \boldsymbol{u}_{abc}$. The discrete-time state-space model of the drive used by the MPC algorithm as prediction model is then

$$\boldsymbol{x}(k+1) = \boldsymbol{A}\boldsymbol{x}(k) + \boldsymbol{B}\boldsymbol{u}(k) \qquad (4a)$$
$$\boldsymbol{y}(k) = \boldsymbol{g}(\boldsymbol{x}(k)). \qquad (4b)$$

The matrices $\boldsymbol{A}$ and $\boldsymbol{B}$ are calculated using exact Euler discretization, i.e., they are of the form $\boldsymbol{A} = \mathrm{e}^{\boldsymbol{E}T_s}$ and $\boldsymbol{B} = -\boldsymbol{E}^{-1}(\boldsymbol{I} - \boldsymbol{A})\boldsymbol{F}$,[1] where $\boldsymbol{E}$ and $\boldsymbol{F}$ are the continuous-time matrices, which can be easily derived from (1). In here, e is the matrix exponential, T_s the sampling interval, and $k \in \mathbb{N}$. The (non)linear function $\boldsymbol{g} : \mathbb{R}^4 \to \mathbb{R}^2$ maps the state variables to the outputs. Depending on the control scheme, the outputs are the stator currents, i.e., $\boldsymbol{y} = \boldsymbol{i}_s$, the torque and stator flux magnitude, i.e., $\boldsymbol{y} = [T_e\ \Psi_s]^T$, or, as proposed here, the torque and rotor flux magnitude, i.e., $\boldsymbol{y} = [T_e\ \Psi_r]^T$.

---

[1]$\boldsymbol{B}$ is time-invariant, thus it can be computed offline. If the computation of $\boldsymbol{A}$ is too computationally intensive, forward Euler approximation can be used instead, i.e., $\boldsymbol{A} = \boldsymbol{I} + \boldsymbol{E}T_s$ and $\boldsymbol{B} = \boldsymbol{F}T_s$. For small sampling intervals T_s and a one-step prediction horizon, forward Euler approximation is sufficiently accurate [2].

III. OBJECTIVE FUNCTIONS

A. MPCC

The block diagram of MPCC can be found in [5, Fig. 4]. The objective function in MPCC is of the form

$$J_1 = J_I + J_{uI}, \qquad (5)$$

with

$$J_I = ||\boldsymbol{i}_s^*(k+1) - \boldsymbol{i}_s(k+1)||_2^2, \qquad (6a)$$
$$J_{uI} = \lambda_{uI}||\Delta\boldsymbol{u}_{abc}(k)||_1, \qquad (6b)$$

where $\boldsymbol{i}_s^*$ is the stator current reference and $\Delta\boldsymbol{u}_{abc}(k) = \boldsymbol{u}_{abc}(k) - \boldsymbol{u}_{abc}(k-1)$ is the difference between two consecutive switch positions. As shown in [5, Appendix A], (5) minimizes the stator current distortions (via J_I) and the switching frequency (via J_{uI}). The trade-off between the two terms is set by the weighting factor $\lambda_{uI} \in \mathbb{R}^+$.

With the proposed controller, the electromagnetic torque and the machine magnetization are controlled *indirectly* through the stator currents. More specifically, based on the reference values of the electromagnetic torque T_e^* and rotor flux magnitude Ψ_r^*, the reference current $\boldsymbol{i}_s^*$ is set by an outer control loop based on the field-oriented control principle [8].

B. MPFC

Because the stator currents relate to the machine flux linkages through

$$\boldsymbol{i}_s = \frac{1}{D}(X_r\boldsymbol{\psi}_s + X_m\boldsymbol{\psi}_r), \qquad (7)$$

(5) can be written as

$$J_1 = J_{I_1} + J_{I_2} + J_{uI}, \qquad (8)$$

where

$$J_{I_1} = \left(\frac{X_r}{D}\right)^2 ||\boldsymbol{\psi}_s^*(k+1) - \boldsymbol{\psi}_s(k+1)||_2^2, \qquad (9a)$$
$$J_{I_2} = \left(\frac{X_m}{D}\right)^2 ||\boldsymbol{\psi}_r^*(k+1) - \boldsymbol{\psi}_r(k+1)||_2^2. \qquad (9b)$$

Owing to the long rotor time constant, it holds that $\boldsymbol{\psi}_r^*(k+1) \approx \boldsymbol{\psi}_r(k+1)$, thus $J_{I_2} \approx 0$. We define

$$J_2 = J_{I_1} + J_{uI}, \qquad (10)$$

which is approximately equal to J_1. J_2 gives rise to model predictive (stator) flux control (MPFC), as discussed, e.g., in [9].

C. Proposed MPTFC

To control the torque and machine magnetization directly, we propose an MPTFC scheme with the objective function

$$J_3 = J_T + J_\Psi + J_{uT}, \qquad (11)$$

where

$$J_T = \lambda_T\left(T_e^*(k+1) - T_e(k+1)\right)^2, \qquad (12a)$$
$$J_\Psi = (1 - \lambda_T)\left(\Psi_r^*(k+1) - \Psi_r(k+1)\right)^2, \qquad (12b)$$
$$J_{uT} = \lambda_{uT}||\Delta\boldsymbol{u}_{abc}(k)||_1, \qquad (12c)$$

$\lambda_T \in [0,1]$, and $\lambda_{uT} \in \mathbb{R}^+$. Due to the slow dynamic of the rotor flux, a one-step horizon does not suffice to achieve

closed-loop control of it. To address this issue, the rotor flux is controlled through the stator flux with [2, (3.70)]

$$\Psi_r = \frac{X_m}{X_s}\cos(\gamma)\Psi_s\,, \tag{13}$$

where γ is the load angle. Consequently, J_Ψ is rewritten as

$$J_\Psi = (1-\lambda_T)\left(\frac{X_m}{X_s}\right)^2 \Big(\cos\big(\gamma^*(k+1)\big)\Psi_s^*(k+1)- $$
$$-\cos\big(\gamma(k+1)\big)\Psi_s(k+1)\Big)^2\,, \tag{14}$$

where $\Psi_s(k+1) = \sqrt{\psi_{s\alpha}^2(k+1)+\psi_{s\beta}^2(k+1)}$. The predicted load angle $\gamma(k+1)$ can be found as follows. With (3) and (7), the electromagnetic torque is rewritten as

$$T_e = \frac{1}{\mathrm{pf}}\frac{X_m}{D}\boldsymbol{\psi}_r\times\boldsymbol{\psi}_s = \frac{1}{\mathrm{pf}}\frac{X_m}{D}\Psi_r\Psi_s\sin(\gamma)\,. \tag{15}$$

It follows that

$$\gamma(k+1) = \arcsin\left(\mathrm{pf}\,\frac{D}{X_m}\frac{T_e(k+1)}{\Psi_r(k+1)\Psi_s(k+1)}\right)\,, \tag{16}$$

where the predicted rotor flux magnitude $\Psi_r(k+1)$ can be computed in a straightforward manner based on (4a) and (7).

As for the references in (14), the desired value of the stator flux magnitude Ψ_s^* is computed by considering (13) and (15), where Ψ_r and T_e are replaced by their references, Ψ_r^* and T_e^*, respectively. Specifically, by squaring both expressions and using the identity $\cos^2(\gamma)+\sin^2(\gamma)=1$, it can be shown that

$$\Psi_s^* = \frac{\sqrt{\big(\mathrm{pf}\,D\,T_e^*\big)^2+\big(X_s\,\Psi_r^{*2}\big)^2}}{X_m\,\Psi_r^*}\,. \tag{17}$$

Finally, the reference of the load angle γ^* is given by (16) where T_e^*, Ψ_r^* and Ψ_s^* are used instead of T_e, Ψ_r and Ψ_s, respectively. As can be understood from the above, the stator flux magnitude reference used in the MPC algorithm is not predefined, but rather derived based on the desired torque and rotor flux magnitude values. This is in contrast to the conventional model predictive torque control, see, e.g., [1], and DTC [3].

The block diagram of the proposed MPTFC can be found in [5, Fig. 2], with the small but crucial difference that the input signals to the controller are T_e^* and Ψ_r^* instead of T_e^* and Ψ_s^*.

IV. OPTIMIZATION PROBLEM

The optimization problem underlying MPCC, MPFC and MPTFC with the objective functions (5), (10) and (11), respectively, is

$$\begin{aligned}
\underset{\boldsymbol{u}_{abc}\in\mathbb{U}}{\text{minimize}}\quad & J_p \\
\text{subject to}\quad & (4),\,(3),\,(7) \\
& \|\Delta\boldsymbol{u}_{abc}(k)\|_\infty \le 1\,,
\end{aligned} \tag{18}$$

where $p\in\{1,2,3\}$ refers to the chosen objective function. The last constraint—the switching constraint—prevents switching transitions between 1 and -1. Owing to its small size, problem (18) can be solved with any off-the-shelf solver for integer programs, including brute-force enumeration [2].
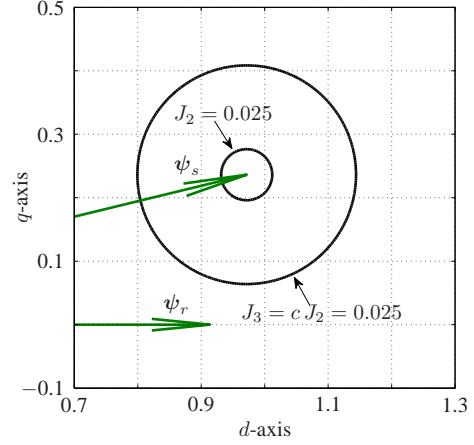

Fig. 2: Level sets of the objective functions J_2, see (10), and J_3, see (11), for the cost value 0.025. For simplicity, we assume that no switching transition occurs from time-step $k-1$ to k, i.e., $\|\Delta\boldsymbol{u}_{abc}(k)\|_1 = 0$.

V. EQUIVALENCE BETWEEN MPCC AND MPTFC

To show the equivalence between MPCC and MPTFC, we will prove in the following that $J_3 = c\,J_2$ with the scaling factor $c = \left(\frac{D}{X_r}\right)^2\frac{(X_m\,\Psi_r^*)^2}{(X_s\,\Psi_r^*)^2+(\mathrm{pf}\,D)^2}$. Because $J_2\approx J_1$, this implies $J_3\approx c\,J_1$ with a negligible difference, as discussed in Section VI.

Consider the dq reference frame with the angular speed $\omega_{\mathrm{fr}}=\omega_s$, where ω_s is the angular stator frequency. Since the transformation from the stationary to the rotating reference frame is amplitude-invariant, the term J_{I_1} in (10)—see (9a)—can be written as

$$J_{I_1} = \left(\frac{X_r}{D}\right)^2 \|\boldsymbol{\psi}_{s,dq}^*(k+1)-\boldsymbol{\psi}_{s,dq}(k+1)\|_2^2\,. \tag{19}$$

The level sets of J_{I_1}—and consequently of J_2—are circles centered at $\boldsymbol{\psi}_{s,dq}^*$, see Fig. 2.

Regarding J_Ψ in (11), the rotor flux magnitude can be written as $\Psi_r = \sqrt{\psi_{rd}^2+\psi_{rq}^2}$. By aligning the d-axis with the rotor flux vector $\boldsymbol{\psi}_r$, (12b) simplifies to

$$J_\Psi = (1-\lambda_T)\big(\psi_{rd}^*(k+1)-\psi_{rd}(k+1)\big)^2\,. \tag{20}$$

Combining (1) and (7), the rotor dynamic with respect to the flux linkages is given by [2, (3.69)]

$$\frac{\mathrm{d}\psi_{rd}}{\mathrm{d}t} = \frac{R_r}{D}\left(X_m\psi_{sd}-X_s\psi_{rd}\right)\,. \tag{21}$$

Given that the derivative of ψ_{rd} must be zero at steady-state operation to maintain the field orientation, it follows that

$$\psi_{rd} = \frac{X_m}{X_s}\psi_{sd}\,. \tag{22}$$

With this, the flux term (12b) is rewritten in terms of the d-component of the stator flux vector

$$J_\Psi = (1-\lambda_T)\left(\frac{X_m}{X_s}\right)^2\big(\psi_{sd}^*(k+1)-\psi_{sd}(k+1)\big)^2\,. \tag{23}$$

For the torque, it follows from (15) that (since $\psi_{rq}=0$)

$$T_e = \frac{1}{\mathrm{pf}}\frac{X_m}{D}\psi_{rd}\psi_{sq}\,. \tag{24}$$

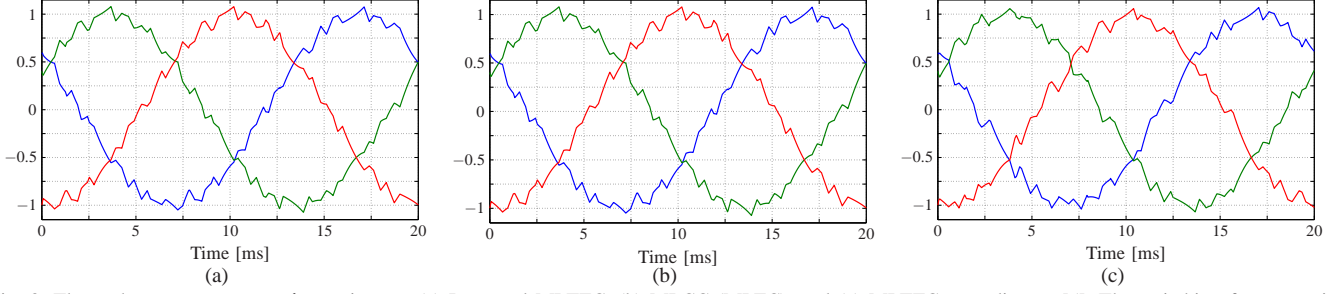As before, we assume that $\psi_{rd}\approx\psi_{rd}^*=\Psi_r^*$. The torque

Fig. 3: Three-phase stator current $\boldsymbol{i}_{s,abc}$ in p.u.. (a) Proposed MPTFC, (b) MPCC (MPFC), and (c) MPTFC according to [5]. The switching frequency is in all cases $f_{\text{sw}} = 250\,\text{Hz}$.
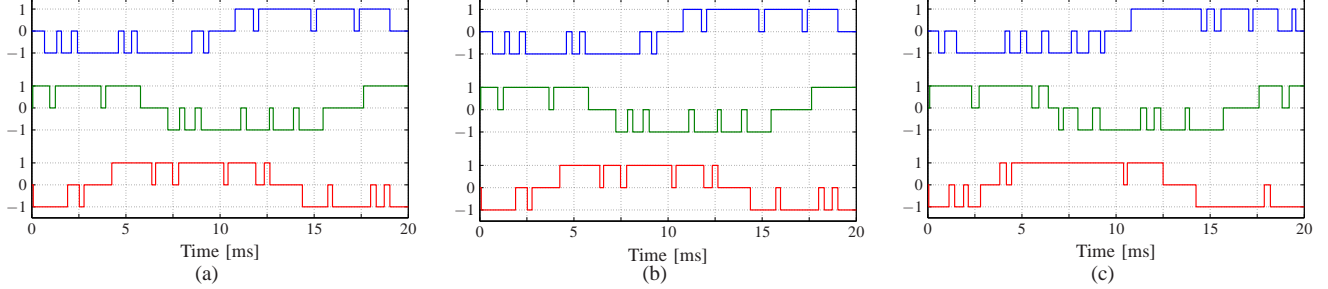

Fig. 4: Three-phase switch position $\boldsymbol{u}_{abc}$ for the cases shown in Fig. 3. (a) Proposed MPTFC, (b) MPCC (MPFC), and (c) MPTFC according to [5].

term (12a) can then be written as

$$J_T = \lambda_T \left(\frac{1}{\text{pf}} \frac{X_m}{D} \Psi_r^* \right)^2 \left(\psi_{sq}^*(k+1) - \psi_{sq}(k+1) \right)^2 . \quad (25)$$

To achieve circular level sets with MPTFC, equal flux errors in the d- and q-axis should result in the same cost. It follows from (23) and (25) that

$$(1 - \lambda_T) \left(\frac{X_m}{X_s} \right)^2 = \lambda_T \left(\frac{1}{\text{pf}} \frac{X_m}{D} \Psi_r^* \right)^2 . \quad (26)$$

The weight on the torque tracking term[2] is thus

$$\lambda_T = \frac{(\text{pf}\,D)^2}{(X_s\,\Psi_r^*)^2 + (\text{pf}\,D)^2} . \quad (27)$$

As a result, the penalties on the torque and flux tracking errors in MPTFC are

$$J_T + J_\Psi = d \left(\left(\psi_{sq}^*(k+1) - \psi_{sq}(k+1) \right)^2 + \right.$$
$$\left. + \left(\psi_{sd}^*(k+1) - \psi_{sd}(k+1) \right)^2 \right) \quad (28)$$
$$= d \,||\boldsymbol{\psi}_{s,dq}^*(k+1) - \boldsymbol{\psi}_{s,dq}(k+1)||_2^2 ,$$

with

$$d = \frac{(X_m\,\Psi_r^*)^2}{(X_s\,\Psi_r^*)^2 + (\text{pf}\,D)^2} . \quad (29)$$

Function (28) yields circular level sets, which are centered at $\boldsymbol{\psi}_{s,dq}^*$, as shown in Fig. 2.

The level sets of MPCC and MPTFC are now both circular. In addition to that, in order to achieve the same control behavior in terms of tracking performance (i.e., current distortions) and control effort (i.e., switching frequency), the ratio between the tracking error and the switching penalty terms must be the same for both control methods, see [5]:

$$\frac{J_T + J_\Psi}{J_I} = \frac{J_{uT}}{J_{uI}} \quad \Rightarrow \lambda_{uT} = d \left(\frac{D}{X_r} \right)^2 \lambda_{uI} \quad (30)$$

---

[2]Note that the chosen value of λ_T differs from that in [5, (28)]. This is due to the different formulation of the torque and flux control problem.

This determines a dependency between their penalties on switching, λ_{uI} and λ_{uT}.

Based on the above, (11) can be written as[3]

$$J_3 = d \,||\boldsymbol{\psi}_{s,dq}^* - \boldsymbol{\psi}_{s,dq}||_2^2 + d \left(\frac{D}{X_r} \right)^2 \lambda_{uI} ||\Delta \boldsymbol{u}_{abc}||_1$$
$$= d \left(\frac{D}{X_r} \right)^2 \left(\left(\frac{X_r}{D} \right)^2 ||\boldsymbol{\psi}_{s,dq}^* - \boldsymbol{\psi}_{s,dq}||_2^2 + \lambda_{uI} ||\Delta \boldsymbol{u}_{abc}||_1 \right)$$
$$= d \left(\frac{D}{X_r} \right)^2 J_2 = c\, J_2 . \quad (31)$$

As can be seen in Fig. 2, if the level sets of J_2 are scaled up by c, then they coincide with those of J_3. This implies that MPTFC achieves the same closed-loop performance as MPCC.

VI. DISCUSSION

To examine the performance of the proposed MPTFC method, an MV drive with a squirrel cage IM with $3.3\,\text{kV}$ rated voltage, $356\,\text{A}$ rated current, $2\,\text{MVA}$ rated power, $50\,\text{Hz}$ nominal frequency and 0.25 p.u. total leakage reactance was considered. The three-level NPC voltage source inverter has the constant dc-link voltage $V_{\text{dc}} = 5.2\,\text{kV}$. The sampling interval was set to $T_s = 25\,\mu s$.

The steady-state performance is assessed in terms of the total demand distortions (TDD) of the stator current, I_{TDD}, and electromagnetic torque, T_{TDD}, for a given switching frequency f_{sw}. The torque weight was chosen in accordance with (27), resulting in $\lambda_T = 0.047$, and the scaling parameter $c = 0.0547$.

For instance, by choosing $\lambda_{uT} = 0.141 \cdot 10^{-3}$ in the proposed MPTFC and by tuning $\lambda_{uI} = 2.578 \cdot 10^{-3}$ according to (30) for MPCC/MPFC, an average switching frequency of $f_{\text{sw}} = 250\,\text{Hz}$ results. For this operating point, the MPTFC

---

[3]To improve readability, the time dependency is omitted.

(a) Current TDD vs switching frequency.
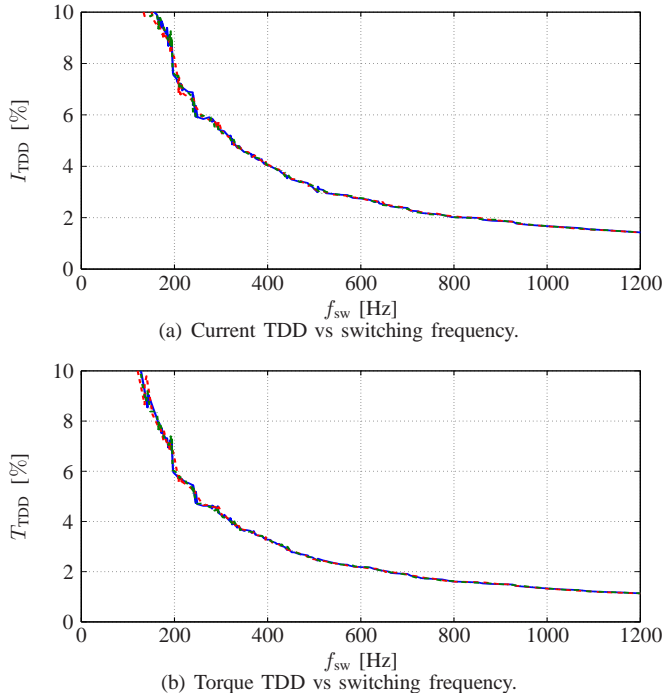

(b) Torque TDD vs switching frequency.

Fig. 5: Trade-off curves of MPCC, MPFC and the proposed MPTFC. MPCC with the objective function J_1 is shown with dashed (red) lines, MPFC with the objective function J_2 relates to the dash-dotted (green) lines, and MPTFC with the objective function J_3 corresponds to the solid (blue) lines.

time-domain waveforms of the stator current and three-phase switch position over one fundamental period are shown in Figs. 3(a) and 4(a), respectively; those of MPCC are shown in Figs. 3(b) and 4(b), respectively (the waveforms of MPFC are the same as for MPCC, and thus omitted). Since the waveforms for all three control methods are identical, the current and torque TDDs are the same; for the specific operating point, they are equal to $I_{\mathrm{TDD}} = 5.87\%$ and $T_{\mathrm{TDD}} = 4.71\%$, respectively.

Following, the switching weight λ_{uT} was varied between $0.02 \cdot 10^{-3}$ and $4 \cdot 10^{-3}$ so as to record a wide range of switching frequencies. More than 200 simulations were run, which are summarized in the trade-off curves shown in Fig. 5. MPTFC was benchmarked in these simulations against MPCC and MPFC. As can be seen, the performance of the proposed MPTFC is identical with that of MPFC. Some minute differences can be observed for MPCC, owing to the assumption that $\psi_r = \psi_r^*$. Nevertheless, for a given state vector, previous switch position, and equivalent current, torque and flux references, MPTFC and MPCC yield the same switch position in 99.4% of the problem instances. The values of their objectives functions—when appropriately scaled by the factor c—differ by at most 10^{-3}, i.e., their relative difference is less than 1%.

This is in contrast to conventional MPTFC based on a constant stator flux magnitude reference [1]. Although the tuning in [5] is done such that the steady-state performance of the torque and flux controller is as close to that of MPCC as possible, the two control schemes are not equivalent. A small but distinct performance difference arises when operating at rated torque and low switching frequencies, see [5, Fig. 10].

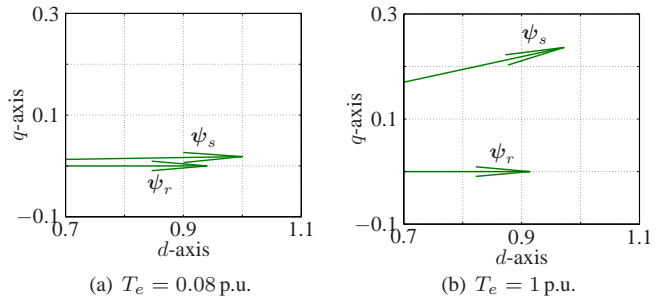(a) $T_e = 0.08$ p.u.

(b) $T_e = 1$ p.u.

Fig. 6: Stator ψ_s and rotor ψ_r flux linkage vectors at (a) low and (b) rated torque. By keeping the stator flux magnitude Ψ_s constant at 1 p.u., the rotor flux magnitude Ψ_r is reduced from 0.94 to 0.91 p.u. when increasing the torque from 0.08 to 1 p.u.

This is also evident from Figs. 3(c) and 4(c), where the stator current and three-phase switch position, respectively, of MPTFC discussed in [5] are depicted. By setting $\lambda_T = 0.052$ according to [5, (28)] as well as $\lambda_{uT} = 0.158 \cdot 10^{-3}$ to achieve $f_{\mathrm{sw}} = 250\,\mathrm{Hz}$ (see [5, (31)]), the resulting current and torque TDDs are $I_{\mathrm{TDD}} = 6.39\%$ and $T_{\mathrm{TDD}} = 5.00\%$, respectively.

Conventional MPTFC [1] and DTC maintain the stator flux magnitude at a constant value, typically 1 p.u. When increasing the torque and thus the load angle γ, the magnitude of the rotor flux vector decreases in accordance with (13). This implies that the machine is (slightly) demagnetized as the torque is increased, as illustrated in Fig. 6. In contrast, owing to the direct control of the *rotor* flux, the proposed MPTFC avoids this demagnetization of the machine at high torque.

VII. CONCLUSION

The proposed model predictive torque and flux controller directly controls the torque and *rotor* flux magnitude of the machine. By appropriately choosing the weighting factors in the objective function analytically, a closed-loop performance closely resembling that of predictive current control is achieved. Consequently, the proposed model predictive torque and flux controller achieves the same low current and torque distortions as predictive current control, without requiring an outer field-oriented controller that sets the current references.

REFERENCES

[1] H. Miranda, P. Cortés, J. I. Yuz, and J. Rodríguez, "Predictive torque control of induction machines based on state-space models," *IEEE Trans. Ind. Electron.*, vol. 56, pp. 1916–1924, Jun. 2009.

[2] T. Geyer, *Model predictive control of high power converters and industrial drives*. Hoboken, NJ: Wiley, 2016.

[3] I. Takahashi and T. Noguchi, "A new quick-response and high-efficiency control strategy of an induction motor," *IEEE Trans. Ind. Appl.*, vol. IA-22, pp. 820–827, Sep. 1986.

[4] J. Holtz, "Advanced PWM and predictive control—An overview," *IEEE Trans. Ind. Electron.*, vol. 63, pp. 3837–3844, Jun. 2016.

[5] T. Geyer, "Algebraic tuning guidelines for model predictive torque and flux control," *IEEE Trans. Ind. Appl.*, pp. 1–12, 2018, early access.

[6] T. Geyer and D. E. Quevedo, "Performance of multistep finite control set model predictive control for power electronics," *IEEE Trans. Power Electron.*, vol. 30, pp. 1633–1644, Mar. 2015.

[7] J. Holtz, "The representation of ac machine dynamics by complex signal flow graphs," *IEEE Trans. Ind. Electron.*, vol. 42, pp. 263–271, Jun. 1995.

[8] F. Blaschke, "The principle of field orientation applied to the new transvector closed-loop control system for rotating field machines," *Siemens Rev.*, vol. 39, pp. 217–220, 1972.

[9] Y. Zhang, H. Yang, and B. Xia, "Model-predictive control of induction motor drives: Torque control versus flux control," *IEEE Trans. Ind. Appl.*, vol. 52, pp. 4050–4060, Sep./Oct. 2016.